Direct Measurement of the Thickness-Dependent Electronic Band Structure of MoS_2 Using Angle-Resolved Photoemission Spectroscopy

Wencan Jin,[1] Po-Chun Yeh,[2] Nader Zaki,[2] Datong Zhang,[1] Jerzy T. Sadowski,[3] Abdullah Al-Mahboob,[3] Arend M. van der Zande,[4,5] Daniel A. Chenet,[5] Jerry I. Dadap,[1] Irving P. Herman,[1] Peter Sutter,[3] James Hone,[5] and Richard M. Osgood, Jr.[1,2,*]

[1]*Department of Applied Physics and Applied Mathematics, Columbia University, New York, New York 10027, USA*
[2]*Department of Electrical Engineering, Columbia University, New York, New York 10027, USA*
[3]*Center for Functional Nanomaterials, Brookhaven National Laboratory, Upton, New York 11973, USA*
[4]*Energy Frontier Research Center, Columbia University, New York, New York 10027, USA*
[5]*Department of Mechanical Engineering, Columbia University, New York, New York 10027, USA*

(Received 26 July 2013; published 3 September 2013)

We report on the evolution of the thickness-dependent electronic band structure of the two-dimensional layered-dichalcogenide molybdenum disulfide (MoS_2). Micrometer-scale angle-resolved photoemission spectroscopy of mechanically exfoliated and chemical-vapor-deposition-grown crystals provides direct evidence for the shifting of the valence band maximum from $\bar{\Gamma}$ to $\bar{K}$, for the case of MoS_2 having more than one layer, to the case of single-layer MoS_2, as predicted by density functional theory. This evolution of the electronic structure from bulk to few-layer to monolayer MoS_2 had earlier been predicted to arise from quantum confinement. Furthermore, one of the consequences of this progression in the electronic structure is the dramatic increase in the hole effective mass, in going from bulk to monolayer MoS_2 at its Brillouin zone center, which is known as the cause for the decreased carrier mobility of the monolayer form compared to that of bulk MoS_2.

DOI: 10.1103/PhysRevLett.111.106801 PACS numbers: 73.22.-f, 73.20.At, 79.60.-i

Molybdenum disulfide (MoS_2) is a layered transition-metal dichalcogenide [1] that can be fabricated as an atomically thin two-dimensional (2D) crystal [2]. The fabrication relies on the fact that S-Mo-S slabs in bulk MoS_2 have a layered 2H crystal structure, and are weakly bonded by van der Waals interactions [3]. After cleaving, monolayer MoS_2 consists of a single layer of Mo atoms sandwiched between two layers of S atoms in a trigonal prismatic structure [4,5]. Our interest in monolayer MoS_2 stems from the following: (i) There is an indirect-to-direct band gap transition in going from multilayer to monolayer crystal due to the missing interlayer interaction in monolayer form [6], and (ii) the strong spin-orbit coupling induced split valence bands ($\sim$160 meV [7,8]) due to broken inversion symmetry, which makes MoS_2 interesting for spin-physics exploration. Properties (i) and (ii) lead to potential applications in nanoelectronic devices [9] and spintronics, respectively. In addition, both properties have been predicted with density functional theory (DFT) calculations [7,10] and indirectly demonstrated using photoluminescence [6,11,12] and Raman spectroscopy [13]. The electronic structure of bulk MoS_2 has been comprehensively studied by both theory and experiments [14–16]. Despite the myriad of experiments on single- and few-layer MoS_2, as well as their distinctive and potential applications, direct experimental determination of the electronic structure of single-to-few-layer MoS_2 crystals has, thus far, been lacking.

In this Letter, we directly measure the electronic band structure of exfoliated monolayer, bilayer, trilayer, and bulk MoS_2, using micrometer-scale angle-resolved photoemission spectroscopy (micro-ARPES), and compare them with the corresponding theoretically predicted bands. The band structure of chemical vapor deposition (CVD)-grown monolayer MoS_2 crystals is also measured and compared to the exfoliated monolayer. The main features of the MoS_2 band structure originate from Mo 4*d* states and are in good agreement with results of theoretical calculations. Our findings show the following: First, the valence bands of monolayer MoS_2, particularly the low-binding-energy bands, are distinctly different from those of few-layer and bulk MoS_2 in that the valence band maximum (VBM) of a monolayer is located at $\bar{K}$ of the first Brillouin zone (BZ), see inset of Fig. 1(b), rather than at $\bar{\Gamma}$, as is the case in bilayer and thicker MoS_2 crystals. Second, the uppermost valence band (UVB) of both exfoliated and CVD-grown monolayer MoS_2 is compressed in energy in comparison with the calculated band, an effect, which we tentatively attribute to interactions with the substrate. The degree of compression in CVD-grown MoS_2 is larger than that in exfoliated monolayer MoS_2, likely due to defects, doping, or stress. Third, the UVB near $\bar{\Gamma}$ of monolayer MoS_2 is less dispersive than that of the bulk, which leads to a striking increase in the hole effective mass and, hence, the reduced carrier mobility of the monolayer compared to bulk MoS_2.

Our measurements were performed on the Spectroscopic Photoemission and Low Energy Electron Microscope (SPELEEM) system at the National Synchrotron Light

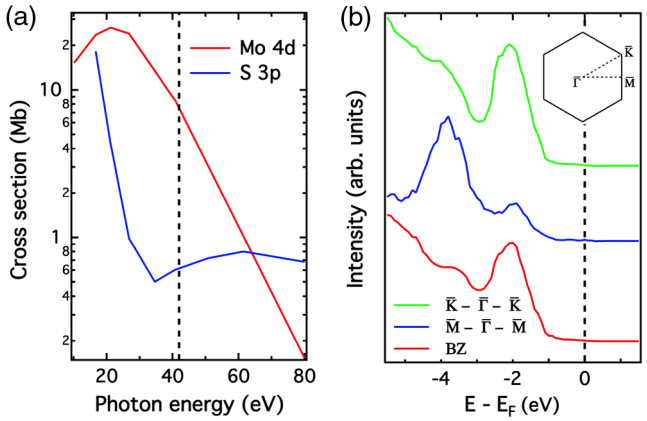

FIG. 1 (color online). (a) Atomic photoionization cross section for Mo $4d$ and S $3p$ subshells as a function of photon energy [21]. The dashed line marks incident photon energy of 42 eV. (b) Angle-integrated photoemission spectra of exfoliated monolayer MoS_2 extracted from high-symmetry directions ($\bar{K}$-$\bar{\Gamma}$-$\bar{K}$ and $\bar{M}$-$\bar{\Gamma}$-$\bar{M}$) of the BZ and over the full BZ. Inset shows the BZ of monolayer MoS_2.

Source (NSLS) beam line U5UA [17,18]. Low energy electron microscope (LEEM) was used to locate the MoS_2 flakes of interest [19]. Each selected MoS_2 flake was characterized with photoemission electron microscopy (PEEM) and microspot low energy electron diffraction (micro-LEED) to investigate surface morphology and crystalline structure, respectively. Micro-ARPES data were collected using synchrotron ultraviolet radiation ($h\nu = 42$ eV) within a 2–5 μm diameter spot, following a procedure described in detail in Refs. [18,20]. Linear-polarized light is incident at an angle normal to the sample surface [19]. Electronic band structure measurements were carried out at room temperature *in situ* with an energy resolution of ~200 meV. The raw data contained photoelectron k-space maps for kinetic energies ranging from 30 to 40 eV at an energy step of 0.1 eV. Projections along high-symmetry directions in the BZ were used to generate band dispersion plots.

The measured valence bands of MoS_2 are derived from hybridization of the Mo $4d$ and S $3p$ orbitals [4,14]. As shown in Fig. 1(a), the calculated atomic photoionization cross section of the Mo $4d$ and S $3p$ subshell as a function of photon energy [21] demonstrates that our incident photon energy is near the Cooper minimum of the S $3p$ orbital. Therefore, the dominant features probed here are derived from Mo $4d$ orbital contributions. As seen in Fig. 1(b), angle-integrated photoemission spectra of exfoliated monolayer MoS_2 were acquired along high-symmetry directions and over the full BZ. These spectra, which were rescaled relative to the intensity at 5-eV binding energy, show a cutoff feature approximately 1.75 eV above the VBM, which we ascribe to the Fermi cutoff (E_F) [22]. Since the band gap of monolayer MoS_2 is ~1.9 eV [11,23], this measurement also indicates that our sample is heavily electron doped, which is consistent with previous reports [2,24,25]. The strong peaks at binding energies of ~2 and ~4 eV, i.e., the main states probed here, can be assigned to Mo $4d$ states, based on a partial-density-of-states decomposition calculation [23].

Figure 2 presents the measured band dispersions of exfoliated monolayer MoS_2 along the $\bar{M}$-$\bar{\Gamma}$-$\bar{K}$ high-symmetry directions of the BZ. As shown in Fig. 2(a), the band structure is generally in good agreement with DFT band calculations with spin-orbit interaction taken into account [7]. In the spectra, the most distinct features include the VBM at $\bar{\Gamma}$ and $\bar{M}$ originating from Mo d_{z^2} orbitals, the VBM at $\bar{K}$ induced by Mo $d_{x^2-y^2}/d_{xy}$ orbitals, and a saddle point at binding energy ~4 eV, as derived from Mo $d_{x^2-y^2}/d_{xy}$ orbitals [15,26]. These features are further displayed in the corresponding energy distribution curves (EDCs) [see Fig. 2(b)] and momentum distribution curves (MDCs) [see Fig. 2(c)]. From matrix-element analysis, the VBM at $\bar{\Gamma}$ has a weak intensity as expected. Other bands, which arise from S $3p$ orbitals and Mo d_{xz}, d_{yz} orbitals [15,26] are too weak to be seen due either to their small cross sections or vanishing matrix elements. Although our energy resolution does not allow us to resolve the spin-orbit splitting near $\bar{K}$, it is apparent that the VBM is located at $\bar{K}$ instead of $\bar{\Gamma}$. A detailed analysis is shown in Fig. 3(a).

Figures 2(d)–2(f) show the evolution of band structure with thickness by displaying the micro-ARPES band maps of bilayer, trilayer, and bulk MoS_2, respectively. The spacing between VBM and E_F is ~1.5 eV, which indicates that our few-layer and bulk MoS_2 samples are also heavily electron doped. A remarkable feature of these few-layer and bulk MoS_2 is that the VBM at $\bar{K}$ are all lower than that at $\bar{\Gamma}$. This striking difference between monolayer and few-layer and bulk MoS_2, thus, provide support for the indirect-to-direct band gap transition in going from few-layer to monolayer MoS_2, as seen in photoluminescence studies [6,11]. This change in electronic structure has been previously ascribed to quantum confinement [6,23]. Note that in multilayer MoS_2, van der Waals interactions allow coupling of the layers and thickness-dependent changes in confinement. Moreover, the VBM at $\bar{\Gamma}$ vanishes due to weak spectral intensity, which has also been reported in bulk MoS_2 experiments by Mahatha *et al.* [16]. Since this state is also derived from the Mo d_{z^2} orbital in few-layer and bulk MoS_2 [26], the weak spectral intensity has been explained as due to the small in-plane lattice parameter of bulk MoS_2 [7], which allows for greater shielding by the S $3p$ orbitals [3].

To fully investigate the thickness dependence of the low-energy dispersive states, we extract the ARPES features of the UVB along the $\bar{M}$-$\bar{\Gamma}$-$\bar{K}$ high-symmetry line by 2D-curvature analysis [27], shown in Figs. 3(a)–3(d). The UVB of exfoliated 1–3 ML and bulk MoS_2 closely match the corresponding calculated bands. These results provide

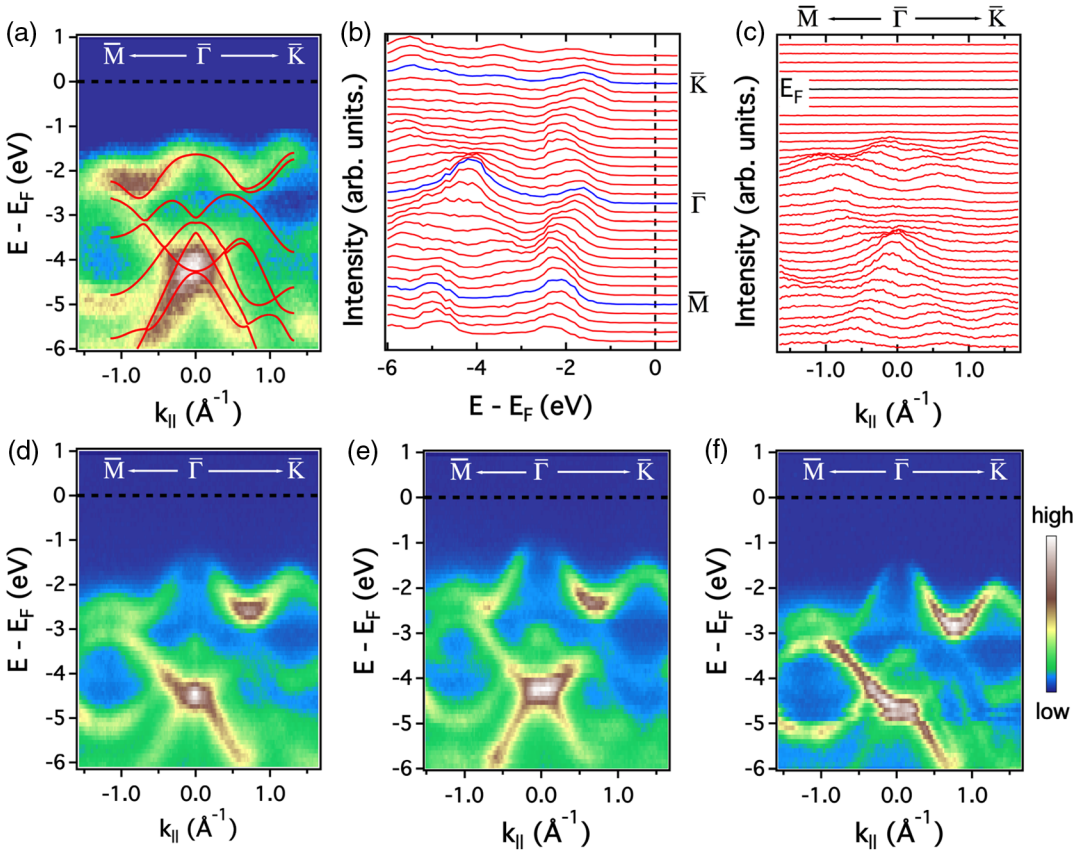

FIG. 2 (color online). (a) ARPES band map of exfoliated monolayer MoS_2 along the $\bar{M}$-$\bar{\Gamma}$-$\bar{K}$ high symmetry lines. DFT band calculations adapted from Ref. [7] (solid red lines) are overlaid onto it for comparison. (b)–(c) Corresponding EDCs and MDCs, respectively. (d)–(f) ARPES band maps of exfoliated bilayer, trilayer, and bulk MoS_2, respectively.

direct experimental evidence for the trend, in which the VBM at $\bar{\Gamma}$ shift upwards in energy relative to that of $\bar{K}$ as the number of layers increases. The thickness dependence of the energy difference between the VBM of $\bar{K}$ and $\bar{\Gamma}$ is further displayed in Fig. 3(e) and compared with theory. This evolution in band structure has been attributed to changes in quantum confinement as the number of layers increases. To be specific, the VBM at $\bar{K}$, which is derived from the localized in-plane Mo $d_{x^2-y^2}/d_{xy}$ orbitals, is unlikely to be affected by the quantum confinement modifications in z direction. By comparison, however, the VBM at $\bar{\Gamma}$, which originates from the rather delocalized out-of-plane Mo d_{z^2} orbitals and S p_z orbitals, is lowered in energy when interlayer interactions decrease in the decreasing number of layers. In addition, one important result is that we reproducibly measure a compression of the UVB in

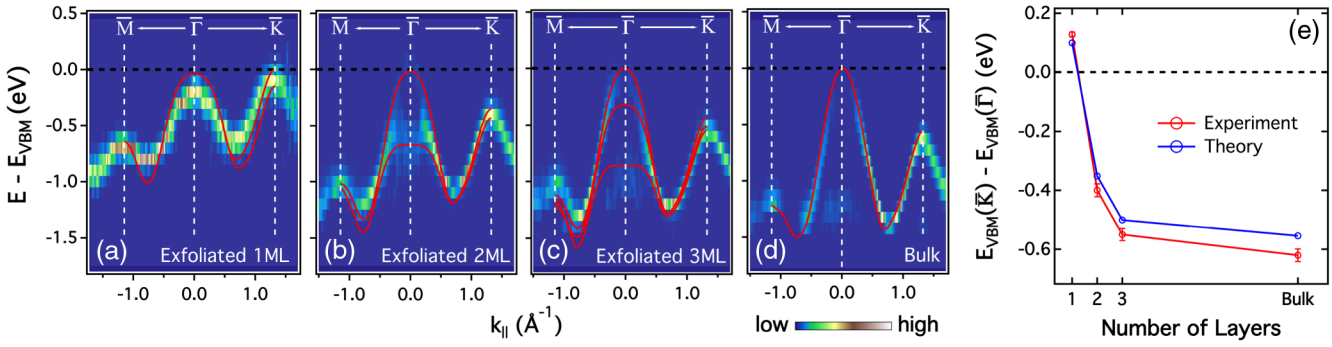

FIG. 3 (color online). (a)–(d) 2D curvature intensity plots of the low energy valence band of exfoliated monolayer, bilayer, trilayer, and bulk MoS_2, respectively. Red curves are the corresponding DFT calculated bands. (e) Thickness dependence of the energy difference between VBM at $\bar{K}$ and $\bar{\Gamma}$. The theoretical and experimental results are plotted together for comparison.

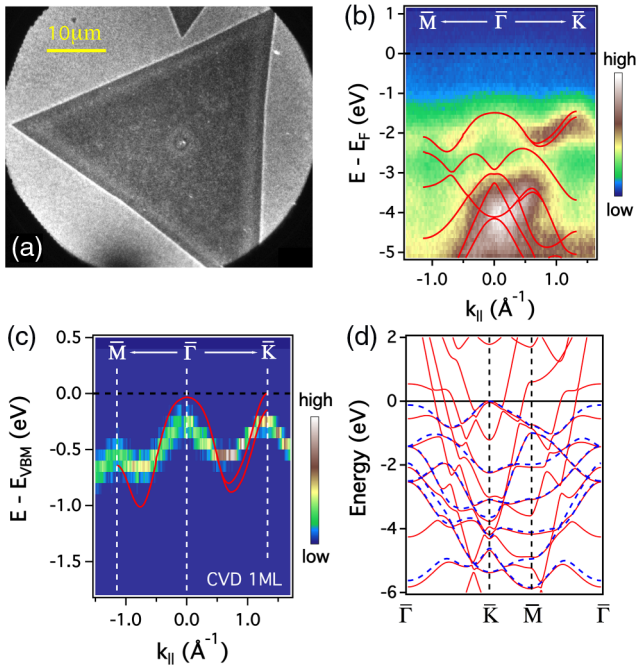

FIG. 4 (color online). (a) PEEM image of a well-defined triangle CVD monolayer MoS_2 island. (b) ARPES band map along $\bar{M}$-$\bar{\Gamma}$-$\bar{K}$ direction. DFT band calculations adapted from Ref. [7] (red curves) are overlaid onto ARPES band map for comparison. (c) 2D curvature intensity plot of the UVB of CVD monolayer MoS_2. The experimental band is shifted in energy to best match the theory. (d) Calculated band structures (red curves) for monolayer MoS_2 on top of *pseudo*-Si. Calculated bands of free-standing monolayer MoS_2 (blue dashed lines) are superimposed onto the hybridized bands for comparison.

monolayer MoS_2, while the rest of the valence bands are identical to the computed bands. Here we define compression as $(\mathrm{UVB_{max}} - \mathrm{UVB_{min}})_{\mathrm{experiment}}/(\mathrm{UVB_{max}} - \mathrm{UVB_{min}})_{\mathrm{theory}}$, where $\mathrm{UVB_{max}}$ and $\mathrm{UVB_{min}}$ are the maximum and minimum values of the UVB. The compression of the monolayer UVB is ~80%. We tentatively attribute this compression to the interaction with the substrate, as confirmed by calculations for MoS_2 on model Si substrate (see below). Another striking effect is that the VBM of monolayer MoS_2 at $\bar{\Gamma}$ is relatively flat compared with its bulk counterpart, indicating a substantially larger effective mass of holes in the monolayer. A simple parabolic fit allows us to estimate the experimental hole effective mass at $\bar{\Gamma}$ of $(2.4 \pm 0.3)m_0$ (m_0 is the electron mass) in monolayer MoS_2, which is in approximate agreement with a theoretical prediction ($\sim 2.8m_0$) [28]. The same fit to the bulk band gives a value of $(0.67 \pm 0.01)m_0$, which is very close to the theoretically predicted value of $0.62m_0$ [28]. From bulk to monolayer MoS_2, the hole effective mass at $\bar{K}$ only slightly increases. The overall hole effective mass of monolayer MoS_2 is thus remarkably larger than that of bulk. This result evidently explains the relatively poor carrier mobility ($< 10\ \mathrm{cm^2/V \cdot s}$) [2,29] of monolayer MoS_2 compared to that of bulk (50–200 $\mathrm{cm^2/V \cdot s}$ at room temperature) [30].

Additionally, we also carried out electronic structure measurements on CVD-grown monolayer MoS_2. Figure 4(a) shows a PEEM image of a well-defined triangular CVD MoS_2 island with a grain size of ~50 μm. The uniform contrast in PEEM confirms that the island used for our ARPES measurements is composed of a high-quality monolayer MoS_2 crystal—except for a very small region of bilayer or multilayer MoS_2 at the center of the triangle [31]. Figure 4(b) shows the band structure of CVD monolayer MoS_2 along $\bar{M}$-$\bar{\Gamma}$-$\bar{K}$. The dispersion generally matches that of the DFT calculations, with the same distinct band features as in the exfoliated case. An unexpected difference between CVD and exfoliated monolayer MoS_2 is that the energy band compression for the CVD MoS_2 is even more pronounced, as shown in the 2D-curvature intensity plot of the UVB [see Fig. 4(c)]. The compression of the UVB for CVD MoS_2 is ~50%. Besides interaction with substrate, the presence of defects, doping, or stress, which are relatively more important in CVD films, may also play a role in the more pronounced compression in the CVD case.

In an attempt to explain the compression of the UVB observed for both exfoliated and CVD monolayer MoS_2, we tested several possible assumptions by conducting preliminary first-principles calculations using the ABINIT code [32,33]. The generalized gradient approximation (GGA) was applied to describe the exchange-correlation potential. We tested two possible causes of band compression: relaxation of atomic positions and MoS_2-substrate interactions. Our structural calculations of monolayer MoS_2, which are obtained by relaxing its atomic positions, indicate that the band structure is very sensitive to relaxation as previously reported by others [10]. For example, a 10% expansion of both a and c lattice spacing can indeed compress the UVB, but it also significantly changes the higher binding energy bands, which, consequently, does not match our experimental observations. Therefore, relaxation is unlikely to be the primary reason for the discrepancy between experiment and theory. With regards to the sample-substrate interaction, we simulated this case by putting monolayer MoS_2 on top of three layers of *pseudo*-Si(111) plane. To simplify the model, we assumed that the lattice parameters of Si(111) are the same as those of MoS_2, thus avoiding the complications of lattice mismatch; a more accurate theoretical model is beyond the scope of this paper. Our calculations shown in Fig. 4(d) indicate that when the spacing between the lower S layer of MoS_2 and the top of the Si layer is set to be 3 Å, the UVB at $\bar{\Gamma}$ is compressed by ~50% while the valence bands at higher binding energy remain nearly unaffected. These results suggest that dielectric interactions with the substrate are likely the main reason for the observed UVB compression in monolayer MoS_2. If indeed this is the case, this opens up one possible route to modifying band dispersion, and with it the hole effective mass and mobility in MoS_2 by way of substrate engineering.

In conclusion, we have used micro-ARPES measurements to probe the valence bands of monolayer MoS_2 derived from the Mo 4*d* orbitals. The results match the DFT predictions generally well and show a striking difference when compared with few-layer and bulk MoS_2. The observed change in the location of the VBM in monolayer MoS_2 provides support for the indirect-to-direct band gap transition in going from few-layer to monolayer MoS_2. The concomitant decrease in the dispersion of the VBM at $\bar{\Gamma}$ leads to a substantially larger hole effective mass, which explains the low hole mobility of monolayer MoS_2 compared to bulk MoS_2.

We acknowledge very useful discussions with Chris A. Marianetti and Philip Kim. This work was financially supported by the U.S. Department of Energy under Contract No. DE-FG 02-04-ER-46157. Research carried out in part at the Center for Functional Nanomaterials and National Synchrotron Light Source, Brookhaven National Laboratory, which are supported by the U.S. Department of Energy, Office of Basic Energy Sciences, under Contract No. DE-AC02-98CH10886. D. Z., A. M. Z., D. C., I. P. H., and J. H. were supported as part of the Center for Redefining Photovoltaic Efficiency through Molecular-Scale Control, an Energy Frontier Research Center funded by the U.S. Department of Energy (DOE), Office of Science, Office of Basic Energy Sciences under Award No. DE-SC0001085.

*osgood@columbia.edu

[1] J. Wilson and A. Yoffe, Adv. Phys. **18**, 193 (1969).
[2] K. S. Novoselov *et al.*, Proc. Natl. Acad. Sci. U.S.A. **102**, 10451 (2005).
[3] T. Böker, R. Severin, A. Müller, C. Janowitz, R. Manzke, D. Voß, P. Krüger, A. Mazur, and J. Pollmann, Phys. Rev. B **64**, 235305 (2001).
[4] L. Mattheiss, Phys. Rev. B **8**, 3719 (1973).
[5] R. Bromley, R. Murray, and A. Yoffe, J. Phys. C **5**, 759 (1972).
[6] A. Splendiani, L. Sun, Y. Zhang, T. Li, J. Kim, C.-Y. Chim, G. Galli, and F. Wang, Nano Lett. **10**, 1271 (2010).
[7] Z. Y. Zhu, Y. C. Cheng, and U. Schwingenschlögl, Phys. Rev. B **84**, 153402 (2011).
[8] D. Xiao, G. B. Liu, W. Feng, X. Xu, and W. Yao, Phys. Rev. Lett. **108**, 196802 (2012).
[9] B. Radisavljevic, A. Radenovic, J. Brivio, V. Giacometti, and A. Kis, Nat. Nanotechnol. **6**, 147 (2011).
[10] W. S. Yun, S. W. Han, S. C. Hong, I. G. Kim, and J. D. Lee, Phys. Rev. B **85**, 033305 (2012).
[11] K. F. Mak, C. Lee, J. Hone, J. Shan, and T. F. Heinz, Phys. Rev. Lett. **105**, 136805 (2010).
[12] K. F. Mak, K. He, J. Shan, and T. F. Heinz, Nat. Nanotechnol. **7**, 494 (2012).
[13] C. Lee, H. Yan, L. E. Brus, T. F. Heinz, J. Hone, and S. Ryu, ACS Nano **4**, 2695 (2010).
[14] R. Coehoorn, C. Haas, J. Dijkstra, C. Flipse, R. de Groot, and A. Wold, Phys. Rev. B **35**, 6195 (1987).
[15] S. W. Han *et al.*, Phys. Rev. B **86**, 115105 (2012).
[16] S. K. Mahatha and K. S. Menon, J. Phys. Condens. Matter **24**, 305502 (2012).
[17] J. I. Flege, E. Vescovo, G. Nintzel, L. H. Lewis, S. Hulbert, and P. Sutter, Nucl. Instrum. Methods Phys. Res., Sect. B **261**, 855 (2007).
[18] P. Sutter, M. S. Hybertsen, J. T. Sadowski, and E. Sutter, Nano Lett. **9**, 2654 (2009).
[19] See Supplemental Material at http://link.aps.org/supplemental/10.1103/PhysRevLett.111.106801 for details about sample preparation, ARPES configuration, and matrix-element analysis.
[20] P. Sutter and E. Sutter, Adv. Funct. Mater. **23**, 2617 (2013).
[21] J. J. Yeh and I. Lindau, At. Data Nucl. Data Tables **32**, 1 (1985).
[22] The value of the Fermi level was also independently confirmed by measuring the photoemission spectrum of the gold grid marks on the substrate and by assuming a lack of a Schottky barrier at the Au/substrate interface.
[23] A. Kuc, N. Zibouche, and T. Heine, Phys. Rev. B **83**, 245213 (2011).
[24] R. S. Sundaram, M. Engel, A. Lombardo, R. Krupke, A. C. Ferrari, Ph. Avouris, and M. Steiner, Nano Lett. **13**, 1416 (2013).
[25] Z. Yin, H. Li, H. Li, L. Jiang, Y. Shi, Y. Sun, G. Lu, Q. Zhang, X. Chen, and H. Zhang, ACS Nano **6**, 74 (2012).
[26] E. Cappelluti, R. Roldán, J. A. Silva-Guillén, P. Ordejón, and F. Guinea, Phys. Rev. B **88**, 075409 (2013).
[27] P. Zhang, P. Richard, T. Qian, Y.-M. Xu, X. Dai, and H. Ding, Rev. Sci. Instrum. **82**, 043712 (2011).
[28] H. Peelaers and C. G. Van de Walle, Phys. Rev. B **86**, 241401 (2012).
[29] A. Ayari, E. Cobas, O. Ogundadegbe, and M. S. Fuhrer, J. Appl. Phys. **101**, 014507 (2007).
[30] R. Fivaz and E. Mooser, Phys. Rev. **163**, 743 (1967).
[31] A. M. van der Zande, P. Y. Huang, D. A. Chenet, T. C. Berkelbach, Y. You, G.-H. Lee, T. F. Heinz, D. R. Reichman, D. A. Muller, and J. C. Hone, Nat. Mater. **12**, 554 (2013).
[32] X. Gonze *et al.*, Z. Kristallogr. **220**, 558 (2005).
[33] X. Gonze *et al.*, Comput. Phys. Commun. **180**, 2582 (2009).